

The Development of a Parameterized Scatter Removal Algorithm for NMIS Imaging

B. R. Grogan^{a,b}, J. T. Mihalcz^a

^aOak Ridge National Laboratory, P.O. Box 2008, MS-6010, Oak Ridge, TN 37831-6010, USA

^bThe University of Tennessee, Department of Nuclear Engineering, 315 Pasqua Engineering Building, Knoxville, TN 37996-2300, USA

Abstract

Neutron radiography is a powerful investigative technique for analyzing the interior structure of an object. If the true attenuation of neutrons at each position in the object can be measured, the attenuation coefficients can be computed and used to identify the materials inside the object. However, scattered neutrons will contribute to the measured neutron flux and reduce the measured attenuation. The Nuclear Materials Identification System (NMIS) uses a time-tagged and electronically collimated D-T neutron source to reduce this effect; however, some of the scattering component remains. This work used Monte Carlo simulations to calculate the scattering component for a variety of scenarios. The scattering for each scenario was fit using a Gaussian distribution to derive a point scatter function. These point scatter functions were used to develop a parameterized scatter removal algorithm that can calculate and remove the scattering component for a wide range of scenarios based on operator inputs. The process used to calculate the scatter functions and develop the scatter removal algorithm is discussed in detail. Examples of simulated and experimental measurements are used to test and validate the algorithm.

Introduction

Neutron radiography seeks to analyze the internal structure of an object (container) by measuring the attenuation of neutrons passing through the object. This is accomplished by measuring the neutron flux using either a position-sensitive detector or multiple smaller detectors. By measuring the neutron flux with and without the object in place, the attenuation, τ , can be calculated using the relationship

$$\tau(x, y) = -\ln\left(\frac{I(x, y)}{I_0(x, y)}\right), \quad (\text{Eq. 1})$$

where x and y represent the detector position, I represents the flux of neutrons with the object in place, and I_0 represents the flux without the object in place. The attenuation is measured in units of mean free paths (MFP), where 1 MFP represents the average distance the neutron travels before interacting [1]. Plotting the attenuation at each (x, y) position yields an attenuation map, or radiograph, of the object. Further, by measuring the attenuation at several different object rotational angles, a full 3D reconstruction of the object attenuation (a tomograph) can be generated. This can also be accomplished using a single projection if cylindrical or spherical symmetry is assumed.

This manuscript has been authored by UT-Battelle, LLC, under contract DE-AC05-00OR22725 with the U.S. Department of Energy. The United States Government retains and the publisher, by accepting the article for publication, acknowledges that the United States Government retains a non-exclusive, paid-up, irrevocable, world-wide license to publish or reproduce the published form of this manuscript, or allow others to do so, for United States Government purposes.

Once the attenuation map of the object is constructed, the attenuation coefficients, μ , of the internal regions can be calculated using the relationship

$$\tau = e^{-\mu \ell}, \tag{Eq. 2}$$

where ℓ is the average path length for a neutron passing through the object to a given detector position. These attenuation coefficients can be used to identify the material in each region of the object. Thus, both the dimensions and composition of each region can be measured using neutron radiography.

Equation 1 assumes that as neutrons interact in the object, they are either absorbed or scattered in such a manner that they fail to reach the detectors. Typically, this assumption is only valid when the object-to-detector distance is much greater than both the size of the object and the width of the incoming neutron beam [2]. In most scenarios, scattered neutrons will contribute a significant fraction of the detected neutron flux. For very thick objects, the scattered neutrons can greatly outnumber the directly transmitted ones.

The Nuclear Materials Identification System (NMIS) conducts neutron radiography measurements using the configuration shown in Figure 1. The object to be imaged is placed on a turntable located between the neutron source and the imaging detectors. The imaging detectors are 32 $2.54 \times 2.54 \times 10.16$ cm plastic scintillators arrayed in a horizontal arc which is centered vertically on the neutron source. Three motors control the imaging process. The first moves the imaging array and the neutron source up and down synchronously in order to capture the full vertical extent of the object. The second motor moves the entire detector array laterally, which allows the object to be imaged multiple times with the detectors at slightly different angles. These images can be overlapped with one another to increase the horizontal resolution of the detector array. The third motor rotates the object so that multiple projections can be taken for full 3D tomographic reconstruction if desired.

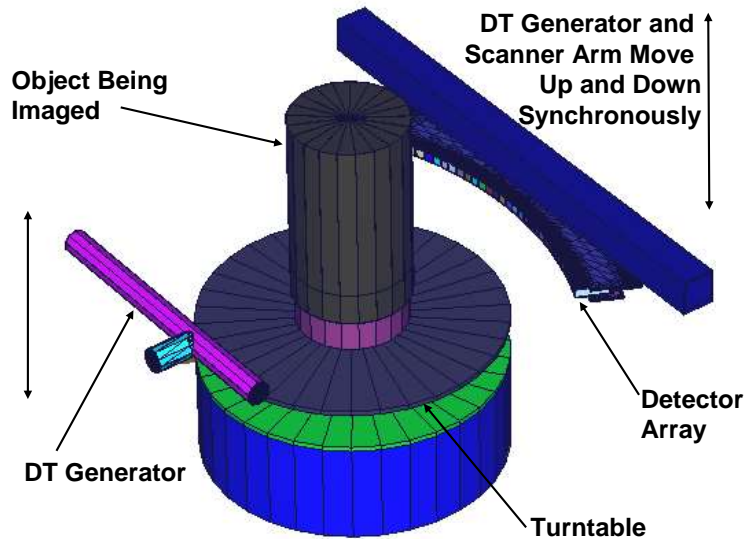


Figure 1. The major components of the NMIS imaging system.

To reduce the contributions of scattered neutrons, NMIS uses an electronically collimated, time-tagged D-T (deuterium-tritium) generator as its neutron source [3]. The D-T generator produces

monoenergetic 14.1 MeV neutrons via the ${}^3\text{H}({}^2\text{H},\text{n}){}^4\text{He}$ reaction. Because the alpha particle and the neutron travel away from the reaction site essentially back-to-back, a cylindrical alpha particle detector can be used to electronically collimate the neutrons into a cone travelling in the opposite direction. The neutrons are further collimated by coupling a pixelated photomultiplier tube to the alpha particle detector. When a single horizontal row of pixels is used, it produces several small horizontal cones of neutrons, each of which is centered vertically on the detector array. The time of each alpha particle's arrival is recorded with 1 ns accuracy. Because the neutrons are monoenergetic, many scattered neutrons can be eliminated by restricting the transmitted neutron signal to a narrow (5 ns) window corresponding to the time-of-flight of the neutrons from the D-T generator to the imaging detectors.

While these techniques greatly reduce the contribution of scattered neutrons to the measured signal, some scattered neutrons are still misidentified as directly transmitted. In particular, heavy metals accentuate the scattering because they preferentially forward scatter the neutrons with little loss of energy. The scattered neutrons systematically lower the measured attenuation, which can result in the misidentification of the materials in the object. To correctly identify the materials, the fraction of scattered neutrons that are misidentified as directly transmitted needs to be calculated and subtracted from the measured values. This paper details a technique for estimating the scattering component and removing it from the measured values using an iterative method.

Methodology

The MCNP-PoliMi code was used to simulate the scattering contribution in NMIS measurements. This code is a modified version of MCNP-4c that attempts to model each neutron-nucleus interaction as accurately as possible [4]. In addition, the program produces an output file that records information such as the time, type of interaction, and energy imparted by each interaction in the detector cells. A post-processor can then use this data to determine which interactions would be able to exceed the detector threshold and register as a count in the NMIS software. Simultaneously, the counts produced by directly transmitted neutrons can be identified so that the scattering component can be extracted.

The first step towards developing a scattering algorithm applicable to general objects was to develop a library of the scatter in simple, homogeneous objects. The shape chosen was an annular arc of material centered on the D-T target spot (the point where neutrons are generated.) Because the arc of the detector array is also centered on the D-T target spot, the minimum distance between the object and the detector array remains constant with angle. Four different materials (polyethylene, graphite, iron, and lead) were modeled, and for each, a wide range of thicknesses and object-to-detector distances was simulated. The front face of the modeled detector array is located 110 cm from the D-T target spot. The neutrons are collimated horizontally so that only those incident on a single detector (the target detector) in the center of the array are used. By limiting the source to neutrons directed towards a single detector, it is possible to isolate the neutrons being scattered into each of the detectors in the array due to neutrons directed towards the target detector. Although the neutrons are collimated horizontally, no vertical collimation is performed because neutrons directed above and below the target detector can also scatter back into the array and contribute to the scattering. The resulting neutron profile is a vertical fan that is only one detector wide but has the full vertical extent of the D-T pixels. This configuration is shown in Figure 2.

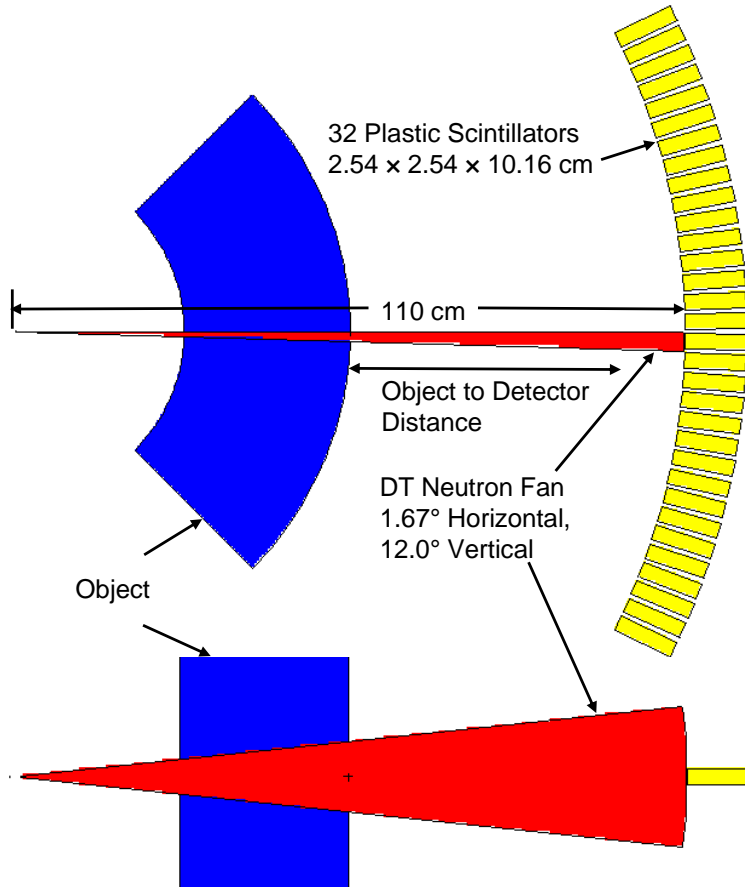


Figure 2. The geometry used for simulating neutron scattering in objects. The neutrons have been collimated into a beam that is directed towards a single detector in order to isolate the scattering into other detectors due to neutrons directed toward the original one.

For each simulation, the number of neutrons scattered into each of the detectors in the array was recorded. These values were used to produce a point scatter function (PScF), which represents the number of additional counts in the transmission timing window due to scattered neutrons in a detector located at an angle θ from the target detector per incident neutron. The PScF concept has been used in the past to remove scatter from measurements using much simpler imaging geometries [5–7]. In addition, a single inter-array scatter function (ISF) was recorded using a void simulation. The ISF represents neutrons scattered from one detector into another without generating sufficient light to generate an electronic pulse. Neutrons that generate a pulse in both detectors (cross-talk) can be eliminated using an anti-coincidence algorithm in the MCNP-PoliMi post-processor and do not contribute to the ISF.

For each object configuration, the PScF was fit and parameterized (maximum, angular standard deviation) using a Gaussian function. The maximum and standard deviation parameters of the Gaussian functions were then fit using the thickness and object-to-detector distances as input variables. Each of the inputs was fit simultaneously using multivariate methods. The fits were made using the JMP 7 statistical software [8]. These fits produced a series of equations that can determine the best PScF to use for a particular object, even if the configuration was not one of the ones originally modeled. These functions are referred to as PScF generating equations (PScFGEs).

To remove the scatter from measured values, a parameterized scatter removal algorithm (PSRA) was developed. The PSRA generates the PScF resulting from neutrons incident on each of the detectors in the array based on operator inputs for the material and object-to-detector distance, and the measured attenuation values. The full details of the PSRA development and implementation can be found in [9].

Results

Initial testing of the PSRA used MCNP-PoliMi simulations. This allowed for testing of the PSRA algorithm separate from any considerations of how accurately the simulations were modeled. In the interest of brevity, only a single simulation result is presented here. The object in this scenario is an iron step wedge. The step wedge is composed of slabs of iron varying between 1 and 3.5 MFP thick, where 1 MFP is approximately 4.6 cm. The position of the step wedge relative to the detector array and the source location is shown in Figure 3.

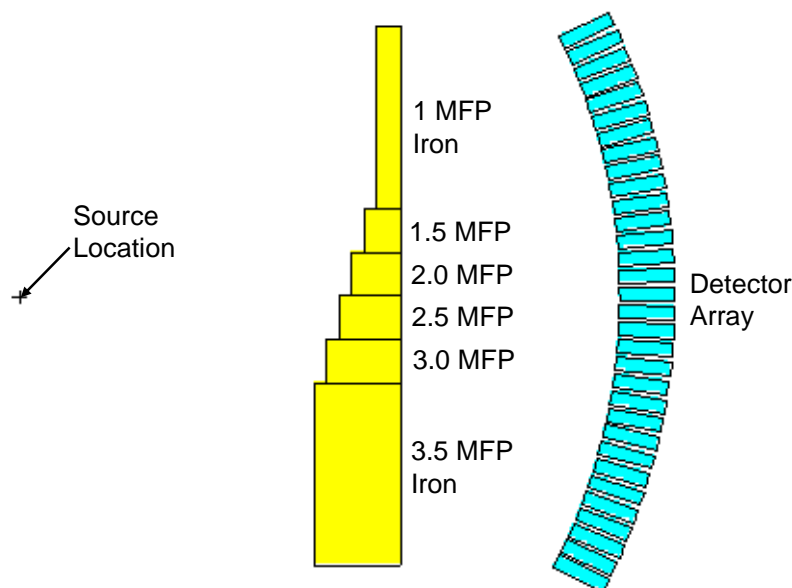


Figure 3. The configuration of the iron step wedge model.

The attenuation curves resulting from the step wedge simulation are shown in Figure 4. These curves represent the attenuation of D-T neutrons through in the step wedge as a function of detector angle. The “direct” attenuation curve was generated using only the directly transmitted neutrons. The uncorrected values show how neutron scattering results in a systematic underestimation of the attenuation values. This underestimation grows worse as the thickness increases. The corrected values match the direct attenuation values very well, with only a very slight deviation at the two greatest thicknesses. The small peak at $\sim 25^\circ$ is due to poor statistics because very few of the D-T neutrons are directed towards the edges of the array. A χ^2 goodness of fit using the direct values as a baseline shows that the corrected χ^2 value is 521 times smaller than the uncorrected one. This result (and others presented in [9]) shows that the PSRA methodology is valid and can produce reliable results.

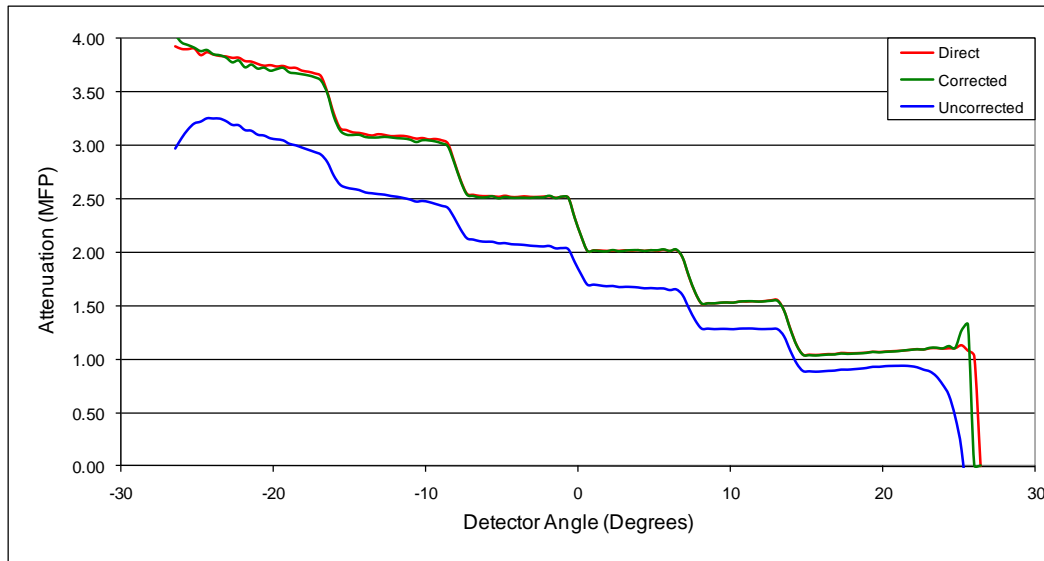


Figure 4. The attenuation curves for the iron step wedge. The “direct” values were calculated using only directly transmitted neutrons. The uncorrected curve systematically underestimates the attenuation. After the PSRA is applied, the corrected values follow the “direct” values very closely. Vertical error bar widths are on the order of the line thicknesses for all three curves and are omitted for clarity.

As with the simulations, only a single measurement is presented here due to space limitations. The object chosen for this measurement is a barrel filled with steel shot, iron pipes, a depleted uranium (DU) casting, and a polyethylene rod. This configuration was designed to create an object that primarily consists of heavy metals to accentuate the forward scattering of neutrons. A picture of the barrel and its contents is presented in Figure 5. The dimensions and composition of the interior regions are listed in Table 1 along with the attenuation values of the materials.

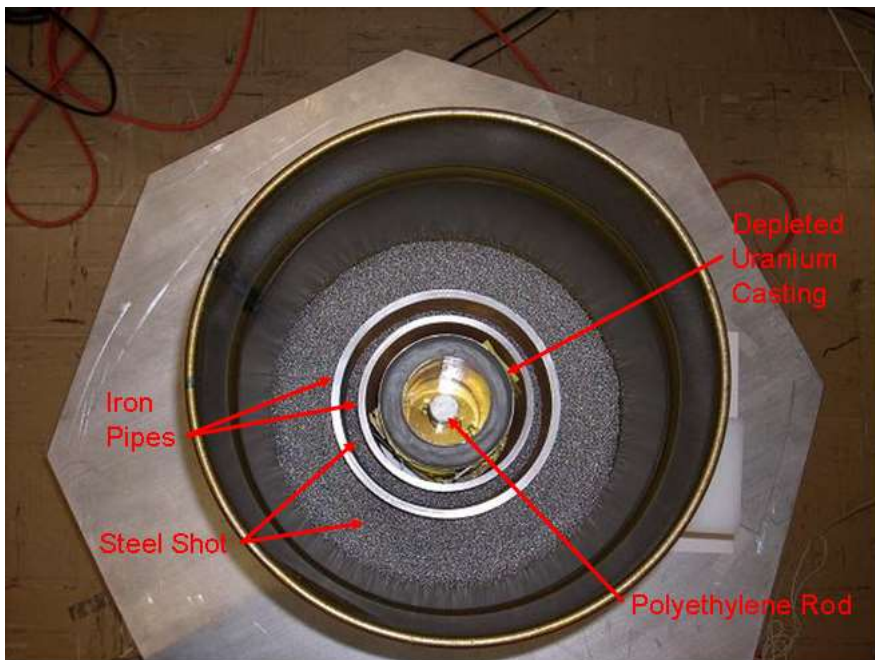


Figure 5. A barrel filled with steel shot, iron pipes, a DU casting, and a polyethylene rod. This object was selected for imaging because the heavy metals inside accentuate the forward scattering of neutrons.

Table 1. The dimensions and compositions of the shells of material inside of the barrel

Shell	Material	Inside Diameter (cm)	Outside Diameter (cm)	Attenuation Coeff. (cm ⁻¹)
1	Polyethylene	0	2.54	0.11
2	Air	2.54	8.89	0.00
3	Depleted uranium	8.89	12.70	0.28
4	Air	12.70	15.24	0.00
5	Iron pipe	15.24	16.83	0.22
6	Steel shot	16.83	20.32	0.13
7	Iron pipe	20.32	21.91	0.22
8	Steel shot	21.91	35.56	0.13

The initial application of the PSRA to the measured values showed an improvement over the initial uncorrected values, but they failed to entirely remove the scattering effect. The most likely cause of this under correction is that the initial MCNP-PoliMi simulations underestimated the scattering present in the experimental measurements. A multiplicative factor of 1.55 was found to produce satisfactory results for all imaging measurements [9].

A filtered back projection (FBP) was performed using both the uncorrected (measured) values and the corrected (after applying multiplicative factor) attenuation values. The FBP assumes that the object in question is cylindrically symmetric. These FBP are shown in Figure 6. In the uncorrected image (left), there is insufficient contrast to discern the two iron pipes from the steel shot. Also, the difference between the attenuation coefficients of the DU casting and the steel shot are nearly imperceptible. In the corrected FBP (right), the DU casting clearly has a higher attenuation coefficient than any of the other regions. The outer iron pipe is clearly distinguishable from the beads on either side. This represents a substantial improvement in contrast, which would allow the operators to identify the composition and dimensions of the various regions inside the object with greater accuracy than without the PSRA correction.

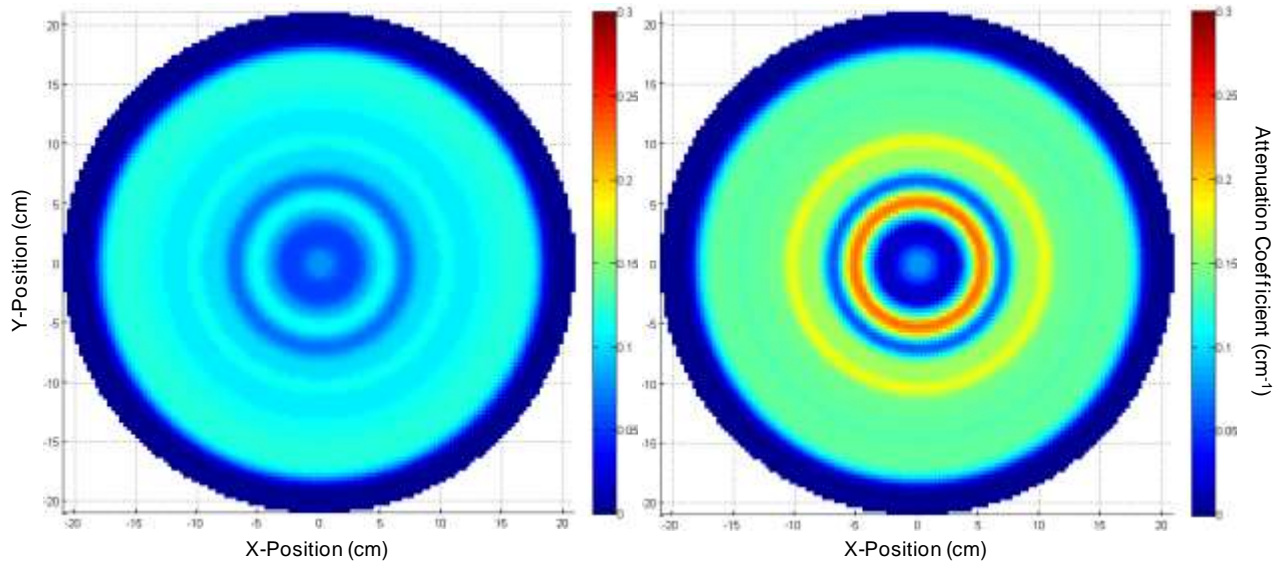


Figure 6. Filtered back projections of the (left) measured and (right) corrected attenuation curves produced by the barrel measurement. The corrected image shows a much higher contrast between regions of different materials than the uncorrected values.

Conclusions

This work has shown that the iterative PSRA methodology can successfully remove the scattered neutron contribution from simulations. This result confirms that the method itself is sound. Although the correction of simulations produced excellent results, the application of the PSRA to experimental results under corrected the scattering. The most likely cause of this under correction is a lack of fidelity in the original models used to calculate the PScFs. If the scattering in the experimental measurements can be modeled more accurately, the PSRA should be able to produce attenuation values that are much more accurate than the measured ones. This will improve the ability to identify the dimensions and material composition of the regions inside the object being imaged.

References

1. J. K. Shultis and R. E. Faw, *Radiation Shielding*, Prentice-Hall, Upper Saddle River, NJ, 1996.
2. J. E. Turner, *Atoms, Radiation, and Radiation Protection*, 2nd Edition, John Wiley & Sons, New York, 1995.
3. P. A. Hausladen et al., “Portable fast neutron radiography with the nuclear materials identification system for fissile material transfers,” *Nuclear Instruments and Methods in Physics Research B* **261**, 387-390 (2007).
4. E. Padovani and S. A. Pozzi, *MCNP-PoliMi Ver. 1.0 Users Manual*, CESNEF-021125, Polytechnic of Milan, Italy, 2002.
5. N. Kardjilov et al., “Representation of the image formation in applied neutron radiography in terms of a PSF superposition,” *Applied Physics A* **74** (Suppl.), S228–S230 (2002).
6. René Hassanein et al., “Methods of scattering corrections for quantitative neutron radiography,” *Nuclear Instruments and Methods in Physics Research A* **542**, 353–360 (2005).
7. M. H. Hassan, “Point Scattered Function (PScF) for fast neutron radiography,” *Nuclear Instruments and Methods in Physics Research B* **267**, 2545–2549 (2009).
8. SAS Institute, *JMP User Guide, Release 7*, SAS Institute, Inc., Cary, NC, 2007, http://www.jmp.com/support/downloads/pdf/jmp_user_guide.pdf (accessed November 2009).
9. B. R. Grogan, *The Development of a Parameterized Scatter Removal Algorithm for Nuclear Materials Identification System Imaging*, ORNL/TM-2010/65, Oak Ridge National Laboratory, 2010.